Bremsstrahlung in Electron-Proton Scattering*

E. A. ALLTON†

High-Energy Physics Laboratory, Stanford University, Stanford, California

(Received 25 February 1964)

Measurements were made of the differential cross section for high-energy electron-proton scattering accompanied by either the emission of photons of various energies or low-energy pions. The dominant process studied was scattering of electrons accompanied by the emission of a single hard photon. The experiment was carried out by observing the spectrum of the inelastically scattered electron without observation of the recoil proton or emitted photon. The differential cross section for this process was computed theoretically by the numerical integration of a formula previously obtained by Berg and Lindner. The result of the integration yielded an approximate formula which expresses the cross section in terms of an "equivalent radiator." This formula was checked against both the more accurate computation and the experiment and found to be in good agreement. The theoretical expression for inelastic electron scattering is given in terms of the experimental measurements of elastic electron-proton scattering. The check of experiment against theory could be made insensitive to both the values of the elastic electron-proton cross sections assumed and to the absolute acceptance of the magnetic spectrometer used in the experiment by normalizing the observations to measurements of elastic electron-proton scattering.

I. INTRODUCTION

THE experiment reported below was undertaken initially to identify the background processes underlying pion electroproduction just above threshold; however, the results are important in themselves, and should be of use in the design of future inelastic electron-proton scattering experiments.

The working hypothesis was that the primary phenomenon is bremsstrahlung, the secondary electrons having become inelastic through emission of a single hard photon. If scattering and photon emission take place in a single interaction, we call the process wide-angle bremsstrahlung (WAB). The Feynman diagrams are shown in Figs. 1(a) and 1(b). The differential cross section has been calculated by Berg and Lindner,[1,2] and also by Isaev and Zlatev[3]; the former method of calculation is more convenient for numerical computation and was adopted for use in this experiment.

Because only the scattered electron is detected in this experiment, the Berg-Lindner formula requires integration over the coordinates of the final-state

(a) BETHE-HEITLER   (b) VIRTUAL COMPTON EFFECT

FIG. 1. Feynman diagrams for Berg-Lindner radiative electron scattering.

[1] R. A. Berg and C. N. Lindner, Phys. Rev. 112, 2072 (1958).
[2] R. A. Berg and C. N. Lindner, Nucl. Phys. 26, 259 (1961).
[3] P. S. Isaev and I. S. Zlatev, Nuovo Cimento 13, 1211 (1959).

proton and photon, and it is the integrated result which is referred to as the WAB cross section.

A difficulty arises in connection with the "virtual proton Compton effect" of Fig. 1(b), because the form factors for the virtual photon-proton vertex with the proton virtual are unknown. (These problems are discussed by Berg and Lindner in Ref. 2.) As a first approximation (the "single nucleon approximation" of Berg-Lindner[2]), one can take the proton to be a pure Dirac particle with zero Pauli moment and no pion interactions, and calculate the purely electrodynamic effect of a recoiling radiating proton. When this is done, over the range of energies relevant to the present experiment, the contribution to the WAB cross section from the virtual Compton effect is found to be $\lesssim 1\%$. Because it is unlikely that the virtual pion process will be excited strongly below the pion threshold, it was considered reasonable to neglect all terms except those from the "Bethe-Heitler" diagrams of Fig. 1(a).

The second radiative process contributing to the continuum requires two independent centers, one for "small-angle bremsstrahlung," and another for large-angle (elastic) scattering. The large-angle scattering event must occur on a proton, as the target is so designed that the detector "sees" only liquid hydrogen, but the bremsstrahlung may occur either on a proton or on a nucleus in a target window (Fig. 2). High-energy bremsstrahlung, in general, shows an angular
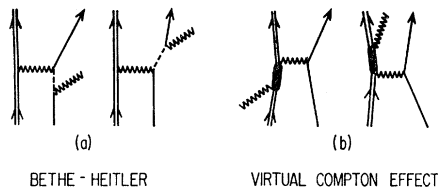

RADIATION BEFORE SCATTERING   RADIATION AFTER SCATTERING
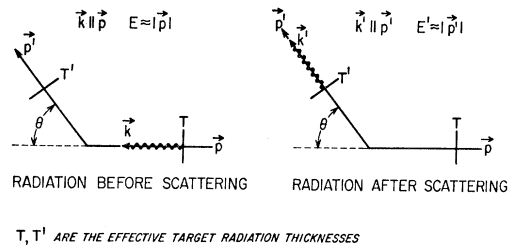
T, T' ARE THE EFFECTIVE TARGET RADIATION THICKNESSES

FIG. 2. Schematic representation of "small-angle bremsstrahlung."

distribution for the electron and photon that is strongly peaked in the forward direction, because of the retardation denominators in the theoretical cross section; the tendency is for both particles to be found in a cone of half-angle $\theta_B \lesssim m/E$ to the original direction, where m and E are the rest mass and relativistic energy of the electron, respectively. The scattering and emission may occur in either sequence.

Because of the smallness of θ_B, this two-step process will be called "small-angle bremsstrahlung" or "SAB."

II. KINEMATICS

An electron e scatters on a proton p, in a reaction of the type

$$e + p \rightarrow e' + X, \tag{1}$$

where only e' is detected, and where X contains, in addition to the recoiling nucleon, any particle or system of particles which may have been created in the process. The experimental design fixes only the initial and final electron energies, E and E', and the scattering angle θ. The kinematic relations are

$$E = \frac{E' + K}{1 - (E'/M)(1 - \cos\theta)}$$

or   (2)

$$E' = \frac{E - K}{1 + (E/M)(1 - \cos\theta)},$$

where M is the proton rest mass. The parameter K is given by

$$K = (W^2 - M^2)/2M,$$

where W is the total relativistic energy of the unobserved system X, as measured in its center-of-momentum system. K is also the laboratory energy required to photoproduce the same system X of energy W, in the reaction

$$\gamma + p \rightarrow X.$$

The change in four-momentum suffered by the electron in the collision, q, gives the Lorentz invariant

$$q^2 \approx -2EE'(1 - \cos\theta), \tag{3}$$

under the approximation $m = 0$. [Note that q^2 does not describe the virtual photon in Fig. 1(a), and is therefore not the argument of the form factors F_1 and F_2 that occur in the Berg-Lindner "Bethe-Heitler" terms.]

III. BREMSSTRAHLUNG CROSS SECTIONS

A. Small-Angle Bremsstrahlung

For incident electron energies $E \gg m$, the largest part of the bremsstrahlung cross section corresponds to both the final electron and the photon traveling along the original line of flight of the radiating electron,

i.e., θ_B is taken to be zero. The resulting kinematics, which must conform to the over-all conditions set by E, E', and θ, are given by

$$E \cdot x \equiv E - k = \frac{E'}{1 - (E'/M)(1 - \cos\theta)}$$

for $\mathbf{k} \parallel$ incident electron direction

and   (4)

$$E'/x' \equiv E' + k' = \frac{E}{1 + (E/M)(1 - \cos\theta)}$$

for $\mathbf{k}' \parallel$ scattered electron direction,

which implicitly defines the energy ratios, x and x'. In each case, the ratio is that of the final to the initial energy, of the radiating electron. The parameters x and x' are convenient for evaluating the Bethe-Heitler "thin-target" bremsstrahlung cross section.

The differential cross section, $(d\sigma/dk)(E,k)$, for an electron of energy E to radiate a photon of energy k when incident on a target nucleus of atomic number Z and atomic weight A g mole^{-1}, may be obtained from the review article of Koch and Motz.[4] In practice, it is convenient to deal with target thicknesses expressed in units of "radiation length," and with the photon number density-in-energy, $N(E,k)$, per radiation length, rather than using $d\sigma/dk$. If $(d\sigma/dk)_0$ represents $d\sigma/dk$ with the "screening parameters"[4] arbitrarily set equal to zero, then a radiation length of l_0 cm of the material of atomic number Z, by definition, contains n_0 nuclei per cm^2 of surface area, where n_0 is a number such that

$$n_0 \int_0^E k \left(\frac{d\sigma}{dk}\right)_0 dk = E.$$

The length l_0 is then

$$l_0 = (n_0/L)(A/\rho) \text{ cm},$$

where L is Avogadro's number and ρ is the density, in g cm^{-3}. We can then define

$$\frac{f(E,x,Z)}{k} \equiv N(E,k,Z) = n_0 \frac{d\sigma}{dk}(E,k,Z) = \left[\frac{l_0 L \rho}{A}\right] \frac{d\sigma}{dk}(E,k,Z),$$

where we have indicated that the bremsstrahlung cross section depends upon the atomic number Z.

Let T and T' be the effective target thicknesses, in units of the radiation length, encountered by the initial and final electron, respectively (Fig. 2). If $T, T' \gg T \cdot T'$, we can make the "one-photon" approximation that the electron radiates in T or in T', but not in both. Taking this approximation together with the "zero angle" approximation involved in (4), we obtain the

[4] H. W. Koch and J. W. Motz, Rev. Mod. Phys. **31**, 920 (1959).

approximate expression for the SAB cross section:

$$\frac{d^2\sigma(E,\theta)}{d\Omega dE'} \approx \frac{Tf(E-k,\,x)}{k}\left(\frac{\partial E}{\partial E'}\right)\frac{d\sigma}{d\Omega}(E-k,\,\theta)$$

$$+\frac{T'f(E'+k',\,x')}{k'}\frac{d\sigma}{d\Omega}(E,\theta),\quad(5)$$

where, from Eq. (4),

$$\partial E/\partial E' = [1-(E'/M)(1-\cos\theta)]^{-2}$$

and $(d\sigma/d\Omega)(E,\theta)$ is the Rosenbluth[5] elastic scattering cross section.

B. Wide-Angle Bremsstrahlung

The WAB cross sections used in this experiment were obtained by numerical integration of the Berg-Lindner formula over photon angles in the center-of-momentum system of the photon and the recoil proton. The problem was programmed in FORTRAN, and executed on the IBM-7090 at the Stanford Computation Center. Copies of the punched card deck and a description of the program are available.

We give the following fairly accurate approximate formula for WAB, identical in form to Eq. (5) and using the same kinematics:

$$\frac{d^2\sigma(E,\theta)}{d\Omega dE'} = \frac{T_0 f_0(x)}{k}\left(\frac{\partial E}{\partial E'}\right)\frac{d\sigma}{d\Omega}(E-k,\,\theta)$$

$$+\frac{T_0 f_0(x')}{k'}\cdot\frac{d\sigma}{d\Omega}(E,\theta).\quad(6)$$

The equivalent radiator is

$$T_0 = (1/137\pi)\{\ln(-q^2/m^2)-1\},$$

while

$$f_0(x) \equiv \tfrac{1}{2}(1+x^2).$$

Equation (6) is obtained from the Berg-Lindner formula by an approximate integration over photon angles in which the relatively slowly varying parts of the integrand are "frozen" at the values they possess when the retardation denominators pass through their minima. This also leads to the kinematics of Eq. (4).

The accuracy of Eq. (6) for the energies of this experiment is shown in Fig. 3. In general, the formula agrees with the accurate integration to within a few percent for secondary energies greater than 50 MeV, angles not much greater than 90°, and values of x greater than 0.5; it becomes asymptotically exact in the limit of soft photons ($x \rightarrow 1$).

A similar formula was derived by Hand,[6] which has a wider range of accuracy than does Eq. (6).

IV. NORMALIZATION TO ELASTIC SCATTERING

The efficiency and effective solid angle of the detector are unknown a priori, but may be derived from the size

and shape of the elastic scattering peak. It is assumed that the angle θ, the nominal secondary energy $\bar{E}'$, and the energy width Δ', centered on $\bar{E}'$, are held at their preset values during any single experimental run, which includes measurements both of the continuum yields and of the elastic yields to which the former are "normalized." In this paper, the term "yield" shall invariably denote the number of counts per 100 (nominal) μC of beam charge which passes through the target and comes to rest on the Faraday cup. The yield is ascertained by measuring the voltage developed by the charge across an integrating capacitor; the accuracy of this measurement is 0.01%. Although the actual charge standard is not precisely 100 μC, it is precisely reproducible, and it therefore cancels in the normalization procedure.

If $R(E')$ is the effective solid angle of the detector (at constant $\bar{E}'$, Δ' and θ), while $\sigma(E,E')$ is the differential cross section for scattering electrons of primary energy E, then the yield is

$$C(E) = \int_{\Delta'} R(E')\sigma(E,E')dE'\quad(7)$$

whether elastic or inelastic scattering is involved. The normalization method effectively solves the integral Eq. (1) for R, given the elastic yields $C_{el}(E)$, and the known elastic scattering cross section, $\sigma(E,E')$.

The range Δ' is divided into n bins, each of width Δ'/n; the bins are numbered from 1 to n in order of increasing energy, and the highest energy in the ith bin is E_i'. In elastic scattering, corresponding to the E_i', are the primary energies

$$E_i = E_i'/[1-(E_i'/M)(1-\cos\theta)].$$

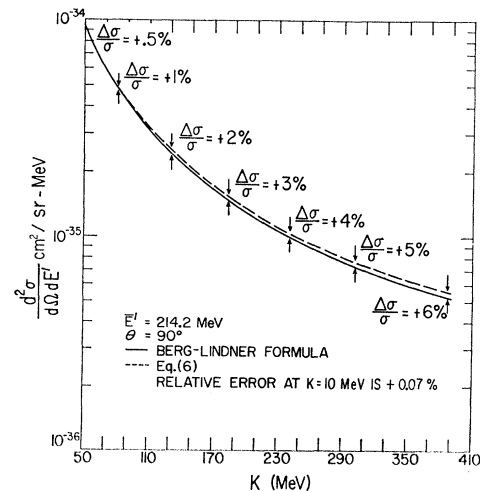For purposes of interpolation, the elastic scattering data $C_{el}(E)$ are fitted to a polynomial, $y(E)$, using the

FIG. 3. Comparison of derived equation with Berg-Lindner formula for WAB.

---

[5] M. N. Rosenbluth, Phys. Rev. 79, 615 (1950).
[6] L. N. Hand, Phys. Rev. 129, 1834 (1963).

method of least squares, weighted with the statistical errors of the data.

In general, the secondary spectrum for a primary beam energy E_i is given by

$$\sigma(E_i, E') = 0, \qquad\qquad E' > E_i'$$
$$\sigma(E_i, E') = \sigma(E_i, \epsilon)\delta(E' - E_i'), \quad E_{i-1} < E' \le E_i \quad (8)$$
$$\sigma(E_i, E') = \sigma_B(E_i, E'), \qquad E' \le E_{i-1}$$

where $\sigma_R(E_i, \epsilon)$ is the Rosenbluth elastic scattering cross section with radiative correction for the finite bin width ϵ, and is given by

$$\sigma(E_i, \epsilon) = (1 - \delta)\sigma_R(E_i, \theta).$$

The fraction lost from the bin by radiation of photons of energy greater than ϵ (emission along scattering direction), or of energy greater than $\epsilon \cdot \eta$ (emission along the beam) is given by Tsai[7] as

$$\delta = X_0\left\{\ln\frac{E_i}{\epsilon\eta} - \frac{13}{12}\right\} + X_0\left\{\ln\left(\frac{E_i'}{\epsilon}\right) - \frac{13}{12}\right\} + \frac{1}{137\pi}\left(\frac{17}{18}\right),$$

where $\eta = (\partial E/\partial E')$, and X_0 is the equivalent radiator for WAB, as in Eq. (6). Terms have been neglected from the virtual Compton effect, as well as one small term containing a Spence function.

The sum of the WAB and SAB differential cross sections is given by $\sigma_B(E_i, E')$, and has the form

$$\sigma_B = \frac{g}{k}\left(\frac{\partial E}{\partial E'}\right) + \frac{g'}{k'},$$

where g and g' are given by

$$g = T_0 f_0(x) + \sum_i T_i f(E - k, x, Z_i),$$
$$g' = T_0 f_0(x') + \sum_j T_j' f(E' + k', x', Z_j).$$

The first term corresponds to WAB, while the summation is over the thicknesses of the various materials making up the composite radiators encountered by the electrons in traversing the target. In the integral Eq. (7), only the photon energies, k and k', vary significantly within one bin width. Using the interpolated counts $y(E)$ and substituting for the $\sigma(E, E')$ in Eq. (7) from Eq. (8) yields the following n equations:

$$y(E_1) = R(E_1')M_{11},$$
$$y(E_2) = R(E_1')M_{12} + R(E_2')M_{22},$$
$$y(E_n) = R(E_1')M_{1n} + R(E_2')M_{2n}$$
$$\qquad\qquad + \cdots + R(E_n')M_{nn}, \quad (9)$$

where the "bin integrals" are

$$M_{jj} = \sigma_R(E_j, \epsilon), \quad j = 1, 2, \cdots n$$

$$M_{ij} = g\ln\left(\frac{E_j - E_{i-1}}{E_j - E_i}\right)$$
$$\qquad + g'\ln\left(\frac{E_j' - E_{i-1}'}{E_j' - E_i'}\right) \quad i = 1, 2, \cdots j - 1.$$

[7] Y. S. Tsai, Phys. Rev. **122**, 1898 (1960).

One now defines the normalization number N as

$$N = \int_{\Delta'} R(E')dE' \qquad (10)$$

and the effective secondary energy,

$$\bar{E}' = \frac{1}{N}\int_{\Delta'} E'R(E')dE'. \qquad (11)$$

The described procedure thus calibrates both the spectrometer sensitivity and the secondary energy $\bar{E}'$.

Assume that the continuum cross section $\sigma(E, E')$ may be expanded as a Taylor's series in $(E' - \bar{E}')$. By virtue of the centroid definition of $\bar{E}'$, the linear terms in $(E' - \bar{E}')$ do not contribute to the integral in Eq. (1), so that to first order in $E' - \bar{E}'$

$$\sigma(E, \bar{E}') \approx C(E)/N. \qquad (12)$$

A special run was made at high secondary resolution, to test whether the normalization procedure was accurately handling the radiative corrections. The general shape of $R(E')$, and the normalization number N, should be unchanged by the addition of 0.05 radiation length of copper foil to T. Yields were obtained at each energy E, with and without the added foil in the incident beam. The resulting $R(E')$ curves were substantially the same, while the two values of N agreed to within 2%.

V. APPARATUS

The experimental arrangement is shown schematically in Fig. 4. The spectrometer is[5] the "zero dispersion" double focusing type, designed by Brown, Rockhold, Alvarez, and Panofsky.[8] Electrons which clear the
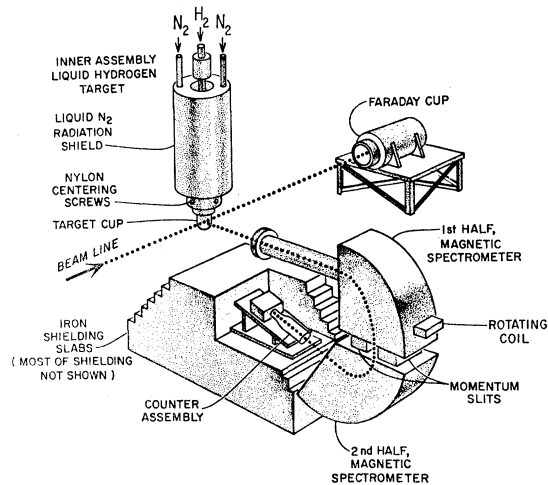

FIG. 4. Experimental arrangement with cutaway showing Čerenkov counter.

[8] R. A. Alvarez, K. L. Brown, W. K. H. Panofsky, and C. P. Rockhold, Rev. Sci. Instr. **31**, 556–564 (1960).

momentum slits are refocused along the counter axis, which decreases the problem of designing the Čerenkov counter.

The Čerenkov counter was designed and built by Hand.[6] It consists of a hollow cylinder, 10 in. long by 5 in. diam, with specular inner side surfaces, and containing paraffin oil. An RCA-7046 phototube was glued to one end of the tube, its face plate forming the wall, in contact with the oil.

The liquid hydrogen target is shown without the scattering chamber, the window foils, or the enveloping vacuum system. The target cup is a vertical cylinder spun out of aluminum, 3.5 in. in diameter, with the wall etched and electropolished down to a thickness of 0.008 in. at beam line. The target required 8 liters of hydrogen to fill from a warm start, and the loss rate in the absence of a beam was one liter in 70 to 80 h.

The Faraday cup stops the beam and holds 99% of the collected charge, which is read as a voltage across an integrating condenser.

The pulses from the phototube are brought to the counting room through 200-Ω low-distortion coaxial lines, and are amplified, discriminated, and counted by scalers. The scalers are generally turned on only during the time in which pulses from prompt events can arrive, through use of a "gating" pulse synchronized to the machine trigger pulse.

VI. EXPERIMENTAL PROCEDURE

As implied earlier, the experiment consisted in measuring the yield $C(E)$ as a function of primary beam energy only, holding $\bar{E}'$, Δ', and θ constant. The basic energy determination, that of E, was made in terms of the original floating wire calibration of the deflecting magnet in the beam switching area of the Mark III accelerator. This calibration was extended to E' through the elastic scattering kinematics and the average 1.49-MeV ionization loss of the primary beam before scattering. Thus, the error in $\bar{E}'$ is not independent of that in E, which is believed to be less than 1%. Reproducibility of both primary and secondary spectrometer energies is assured through use of field measuring devices, so that no additional error is incurred from this source.

The elastic yields provided the normalization number N and the effective secondary energy $\bar{E}'$, as explained above. The inelastic yields were obtained for secondary electrons or positrons at the same values of E and E' through reversing the spectrometer field.

The scalers were arranged in a matrix, all scalers receiving the same signal pulse, but each scaler being served by a separate "gate" pulse related to the accelerator gun pulse. One "early" gate, one "prompt" gate, and several "late" gates, each of one or two microseconds duration were used.

The late gates were arranged to be in accord with the muon half-life, thus allowing possible corrections

for muon decay electron counts from the positive particle yields. One scaler was ungated; it counted only slightly faster than the scaler with the prompt gate.

The counter was checked out by use of a pulse-height analyzer. The distribution of pulse heights showed a very large number of low-voltage pulses and a prominent high-energy electron peak at a higher voltage, having a full width at half-maximum of about 30%. The interval between the peak and the low-voltage pulses contained few or no pulses, indicating a clean separation between signal and noise.

The discriminator bias voltage was adjusted to the low-voltage edge of the electron pulse-height distribution, in order to provide maximum rejection both of high-energy electrons not moving close to the counter axis and of positive pions of the same momentum.

The kinematic constraints of this experiment prevent detection of electrons which have become inelastic by any processes other than bremsstrahlung and electron-positron pair production; it is easy to show that the latter process contributes under 1% of the yield due to the former. Nevertheless, the observed positron yield C^+ is found to range from 0–20% of the electron yield C^- at the same primary energy. If C^+ is attributable entirely to pairs, then the yield of interest is not C^-, but the net yield, $C = C^- - C^+$, assuming equal detection efficiency for positrons and electrons. The primary phenomenon responsible for the large positron yield is evidently conversion in the effective radiator thickness T' of decay photons from π^0 mesons created in hydrogen either by direct electroproduction, or by photoproduction; in either case, the initiating electron scatters forward and is not detected. Such meson production is proportional to the equivalent radiator, T_e,[9] for electroproduction, or to the effective target radiator T, for photoproduction, times the photoproduction cross section, which is several orders of magnitude larger than the Rosenbluth cross section. In either case, one finds electrons emitted at high energy and large angle without the need for large momentum transfer. For these reasons, this mechanism can account for the observed C^+.

TABLE I. Elastic yields. $C(E)$ is number of counts per 100 μC of beam, nominal; $T = 0.0126$ radiation lengths effective; $T' = 0.0073$ radiation lengths effective; $\theta = 90°$; ΔE = average ionization loss = 1.49 MeV; $N = 2.40 \times 10^{36}$ counts per 100 μC per (cm²/sr-MeV); $\bar{E}' = 212.7$ MeV.

E(MeV)	$C(E)$	E	$C(E)$
261.4	77.6±27.6	276.2	17650±740
263.8	3370 ±193	279.9	17600±740
266.3	9790 ±510	284.8	8200±340
271.2	15400 ±715	289.7	2436±158

[9] G. B. Yodh and W. K. H. Panofsky, Phys. Rev. **105**, 731 (1957).

TABLE II. Observed versus predicted yields. $C(E)$ is number of counts per 100 μC of beam, nominal; $\bar{E}'=212.7$ MeV; $\theta=90°$.

E(MeV)	K(MeV)	$C^-(E)$	$C^+(E)$	$C(E)$	Predicted yield	Discrepancy
294.6	15.2	1430±120	0	1430 ±120	1439	−9 ±120
339.6	49.9	334± 18	0	334 ± 18	333	1 ± 18
360.8	66.4	254± 16	16±6	238 ± 17	228	10 ± 17
381.0	82.0	200± 10	29±7	171 ± 12	171	0 ± 12
430.4	120.2	128± 4	33±3	96 ± 5	100	−4 ± 5
505.4[a]	178.2	104± 3	37±2	68.3± 4.0	57.6	10.7± 4.0

[a] Above pion threshold.

However, subtraction of the positron yield can cause an overcorrection if the $\pi^+ \to \mu^+ \to e^+$ decay scheme makes up an important part of the positron yield, since this source has no negatively charged analog in a hydrogen target. For this reason, considerable care was taken to assure that C^+ did not contain an appreciable contamination from π^+ decay. For example, it was necessary to show that π^+ mesons of momentum 214 MeV/c did not produce sufficient Čerenkov light to count directly; this was done by examining the pulse height spectrum for the π^+ peak at low voltage, and biasing the counters well above this level, yet not so high as to lower the electron counting efficiency. The time-spectrum of delayed counts was also obtained in order to estimate the muon flux as a correction for the counting rate in the prompt gate. It is believed that C^+ contains at most 10% contaminant from π^+ activity, which reflects a maximum error of 2% into C, in the form of an underestimate. This estimate sets an upper limit, and it is not unlikely that the true error is much less.

Auxiliary test runs were carried out to show that the beam was free of photons not accounted for in terms of the effective radiator thickness T and that the beam did not have a diffuse halo.

VII. DATA

The yields over the elastic peak, $C_{el}(E)$ versus E, are given in Table I.

The inelastic yields, $C^-(E)$ for electrons, $C^+(E)$ for positrons, and $C(E)=C^--C^+$, are given in Table II.

No counting rate loss corrections were applicable, and empty target yields were consistent with those expected from cold H$_2$ gas.

Figure 5 shows a comparison of the experimental yield curve, $C(E)$ versus E, compared to

$$C'(E)=R(E')\,(d\sigma/d\Omega)\,(E,\theta)$$

versus E, where

$$E'=E\left/\left[1+\frac{E}{M}(1-\cos\theta)\right].\right.$$

The curve $C'(E)$ is fictitious, because it predicts the yield uncorrected for bremsstrahlung in elastic scattering. The discrepancy in areas under these two curves is a rough measure of the over-all radiative correction. Note that the high-energy tail has been removed in $C'(E)$.

VIII. RESULTS AND CONCLUSIONS

The measured inelastic yields, C^- for electrons, C^+ for positrons and $C=C^--C^+$, are presented in Table II, as a function of the primary energy E. The "predicted yield" is obtained by integrating $\sigma=\sigma_{WAB}+\sigma_{SAB}$ over $R(E')$. The discrepancy between the two yields is listed and, with the exception of the yield at $E=505.4$ MeV, is consistent with zero.

The normalized cross sections, Σ^- for electrons, Σ^+ for positrons, and $\Sigma=\Sigma^--\Sigma^+$, are given in Table III. The theoretical cross section is $\sigma=\sigma_{WAB}+\sigma_{SAB}$. The discrepancy is given in the column headed $\Sigma-\sigma$. With the same exception as above, the entries in this column are consistent with zero.

The above-threshold "$\Sigma-\sigma$" is attributed to pion electroproduction. While the error is large, the result
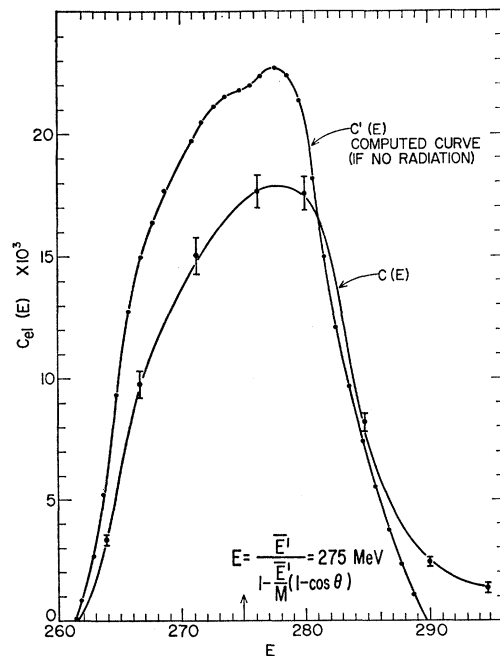

FIG. 5. Comparison of actual yield $C(E)$ with curve computed neglecting bremsstrahlung $C'(E)$.

TABLE III. Measured versus theoretical cross sections. $C(E)$ is number of counts per 100 μC of beam, nominal; $\bar{E}' = 212.7$ MeV; $\theta = 90°$; the cross sections, Σ, σ, are in cm^2/sr-MeV.

E(MeV)	K(MeV)	Σ^-	Σ^+	Σ_{net}	σ	σ_{WAB}	σ_{SAB}	$\Sigma_{net}-\sigma$
294.6	15.2	59.1 ±5.0	0	59.1 ±5.0	58.0	39.8	18.2	1.1 ±5.0
339.6	49.9	13.8 ±0.8	0	13.8 ±0.8	13.9	9.44	4.41	−0.1 ±0.8
360.8	66.4	10.5 ±0.7	0.8 ±0.2	9.86±0.69	9.51	6.45	3.05	0.36±0.69
381.0	82.0	8.28±0.40	1.21±0.29	7.07±0.49	7.12	4.81	2.31	−0.05±0.49
430.4	120.0	5.32±0.16	1.36±0.12	3.96±0.20	4.16	2.79	1.38	−0.20±0.20
505.4[a]	178.2	4.36±0.12	1.53±0.94	2.83±0.16	2.39	1.57	0.81	0.44±0.16

[a] Above pion threshold.

is not consistent with zero, although the $e-\pi$ cross section is seen to constitute but 12% of the total observed cross section at $E = 505.4$ MeV, $K = 178.2$ MeV.

The cross sections are plotted in Fig. 6.

It should be pointed out here that the normalized cross sections are insensitive to the possible experimental errors contained in the primary elastic scattering data. The Rosenbluth cross section at secondary energy $\bar{E}'$, which is a factor in the large term in each of the approximate formulas for WAB and SAB, is effectively cancelled by the normalization procedure. The agreement between theory and experiment is quite good. Actually, the radiative nature of the
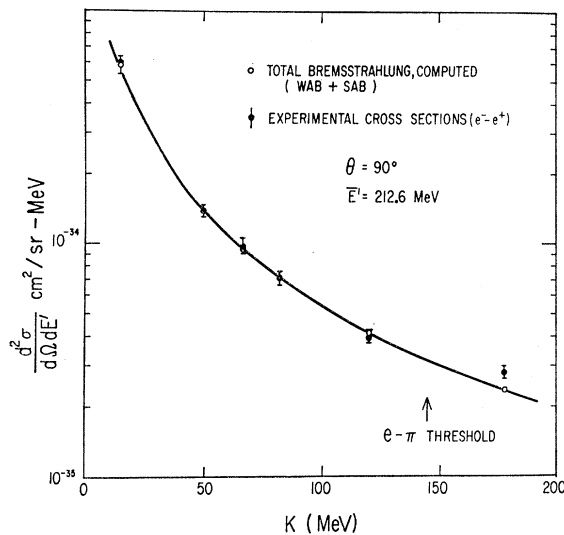

FIG. 6. Experimentally derived cross sections, $d^2\sigma/d\Omega dE'$ versus K.

continuum processes could have been proven simply through the energy dependence of the unnormalized yields. The experiment goes farther, and shows that the normalization procedure obtains the correct scale factor for converting yields into cross sections. In short, the correct energy dependence of the continuum yields proves that we understand the structure of the continuum, while the correct normalization number N shows that we understand the spectrometer and the required radiative corrections to elastic scattering. Both of these factors are important to a successful relative cross section measurement for electroproduction of pions just above threshold.

The most important conclusion, from the standpoint of the pion electroproduction experiment, reported elsewhere, is qualitative: the continuum is shown to depend upon two radiative processes whose cross sections are known from theory.